Nanoscale Research Letters

NANO EXPRESS Open Access

Structure and Dielectric Property of High-*k* ZrO_2 Films Grown by Atomic Layer Deposition Using Tetrakis(Dimethylamido)Zirconium and Ozone

Junqing Liu*, Junpeng Li, Jianzhuo Wu and Jiaming Sun*

Abstracts

High-*k* metal oxide films are vital for the future development of microelectronics technology. In this work, ZrO_2 films were grown on silicon by atomic layer deposition (ALD) using tetrakis(dimethylamido)zirconium and ozone as precursors. The relatively constant deposition rate of 0.125 nm/cycle is obtained within the ALD temperature window of 200–250 °C. The film thickness can be precisely controlled by regulating the number of ALD cycle. The ZrO_2 films formed at 200–250 °C have an O/Zr atomic ratio of 1.85–1.9 and a low content of carbon impurity. ZrO_2 film begins to crystallize in ALD process above 210 °C, and the crystal structure is changed from cubic and orthorhombic phases to monoclinic and orthorhombic phases with increasing the deposition temperature to 350 °C. Moreover, the effect of annealing temperature on dielectric properties of ZrO_2 film was studied utilizing ZrO_2-based MIS device. The growth of the interface layer between ZrO_2 and Si substrate leads to the decrease in the capacitance and the leakage current of dielectric layer in the MIS device after 1000 °C annealing. ZrO_2 film exhibits the relatively high dielectric constant of 32.57 at 100 kHz and the low leakage current density of 3.3×10^{-6} A cm^{-2} at 1 MV/cm.

Keywords: Atomic layer deposition, ZrO_2, Electrical property, Thermal annealing

Background

Gate dielectrics have been a continuous research interest due to their broad applications in nano- and microelectronics [1–3], such as metal oxide films for complementary metal oxide semiconductors (CMOS) [4] and dynamic random access memory (DRAM) [5]. However, the use of the traditional SiO_2 comes to its limit due to the scaling of devices, hence it is urgent to develop next generation of gate dielectrics to replace SiO_2 in semiconductor industry [6, 7]. Recently, alternative metal oxides have been extensively investigated, such as ZrO_2, Ta_2O_5, HfO_2, Nb_2O_5, and TiO_2. In particular, ZrO_2 has been considered as an ideal candidate due to its relatively high dielectric constant and wide band gap, as well as excellent thermal and chemical stability [8, 9].

In the past decade, ZrO_2 film has been successfully synthesized via vacuum-based vapor-deposition routes [8, 10–12] and sol-gel solution-deposition routes [13–15]. Among them, atomic layer deposition (ALD) has distinguished advantages over other routes based on saturated self-limiting surface reactions [16, 17], including thickness controllability, large-area uniformity, low deposition temperature, and structure conformality, which makes ALD play an important role in the fabrication of high-quality dielectric films [18, 19].

Several precursors have been successfully applied for deposition of ZrO_2 films by ALD processes. Kukli et al. reported that ZrO_2 films were grown from ZrI_4 and H_2O-H_2O_2 on *p*-Si(100) substrates using ALD technique. The relative permittivity measured at 10 kHz was

* Correspondence: junqingliu@nankai.edu.cn; jmsun@nankai.edu.cn
Research Center for Photonics and Electronics Materials, School of Materials Science and Engineering & National Institute for Advanced Materials, Nankai University, Tongyan Road 38, Tianjin 300350, China

20–24 in the films deposited at 275–325 °C [20]. Kukli et al. reported that ZrO_2 films were grown by ALD from $ZrCl_4$ and H_2O or a mixture of H_2O and H_2O_2 on Si(100) substrates in the temperature range of 180–600 °C. The films grown at 180 °C contain 5–6 at.% of hydrogen and 4–5 at.% chlorine. The effective permittivity of ZrO_2 films is 13–15, when the ZrO_2 was deposited at 180–210 °C [21]. Putkonen et al. reported that ZrO_2 films were deposited onto (100) silicon substrates by ALD using $Cp_2Zr(CH_3)_2$ (Cp = cyclopentadienyl) and water as precursors at 200–500 °C. The effective permittivity was 12.5 for the 19.0-nm film. The leakage current density in a 1 MV/cm field was about 2.8×10^{-5} A/cm^2 for the 19.0-nm ZrO_2 film [22]. Lamperti et al. reported that ZrO_2 films were deposited on Si (100) substrates by ALD at 300 °C from $(MeCp)_2ZrMe(OMe)$ as Zr precursor and using H_2O or O_3 as an oxygen source. The measured dielectric constant values after 800 °C annealing are $k \sim 24$ and $k \sim 30$ in the films [23]. Previously, the common precursors were $ZrCl_4$ [8, 24] or ZrI_4 [25, 26]. However, low reaction activities of halides lead to high deposition temperatures [27]. Moreover, the formation of corrosive by-products (e.g., HCl) can corrode the films and ALD systems. Recently, metal amides precursors have been regarded as the ideal replacements without corrosive halogen by-products. Moreover, they have much higher reactivity than metal halides, since the metal-nitrogen bond is significantly weaker than the metal-halide bonds. In particular, tetrakis(dimethylamido)zirconium (TDMAZr) has thermal stability [28], sufficient volatility [29], and high reaction activity in the vapor deposition process. Therefore, TDMAZr and H_2O as reaction precursors have been used for ALD processes of ZrO_2 films [30], Nevertheless, hydrogen and carbon impurities in ZrO_2 films have severe effects on the electrical properties of thin films. The "dry" ALD process of metal precursor and ozone (O_3) has attracted more and more interest, because O_3 as oxidizing agent can avoid introducing hydrogen. Moreover, O_3 can remove carbon impurity by forming volatile CO and CO_2 [31]. In addition, O_3 has been widely used in the fabrication of dielectric layer in order to achieve higher crystallinity accompanied by a higher dielectric constant.

In this work, ZrO_2 films were deposited on silicon by ALD technology using TDMAZr as metal precursor and O_3 as oxygen precursor. The dependences of growth rate, refractive index, crystal structure, and surface roughness on deposition temperature were investigated in details by optical ellipsometry, glancing angle incidence X-ray diffraction (GAXRD), X-ray photoelectron spectroscopy (XPS), and atomic force microscope (AFM). Post-deposition annealing was used to further improve the crystal quality of ZrO_2 films. Most importantly, we evaluated the dielectric constant of ZrO_2 film and researched the effect of annealing temperature on the dielectric properties of ZrO_2 films by analyzing the capacitive behavior and leakage current of ZrO_2-based MIS devices.

Methods

ZrO_2 films were grown onto oriented *n*-type silicon wafers using an ALD reactor (MNT Ltd.). High purity nitrogen gas (99.999%) was used as a carrying and purging gas. TDMAZr as metal precursor was heated to 70 °C and carried into a reactor by carrying gas flowing through the source bottle. O_3 as oxidant precursor was generated from oxygen (99.999% purity) by an ozone generator (Newland Ltd.). The delivery lines were remained at 100 °C to keep the gas from condensing. TDMAZr and O_3 entry alternately into the reaction chamber to conduct surface gas-solid chemical reactions. We need to ensure that O_3 is sufficiently excessive (about 20,000 Pa) and the purging process is long enough. The ZrO_2 thin films deposited on silicon were annealed for 2 h under nitrogen atmosphere.

The thickness and refractive index of all samples were measured by an ellipsometer. The crystal structure of ZrO_2 film was analyzed by glancing angle incidence X-ray diffraction (GAXRD). The chemical component and chemical state of ZrO_2 film were analyzed by X-ray photoelectron spectroscopy (XPS, Sigma Probe, ThermoVG) using a monochromatic Al Ka source (1486.7 eV) to excite the photoelectrons. The positions of all the peaks were calibrated with the C 1s peak assigned at 284.6 eV. The surface morphology and the root-mean-squared (RMS) roughness of ZrO_2 film were examined with an atomic force microscope (AFM, JSPM-5200, JEOL Co.). Current-voltage (I–V) measurement was carried out by a Keithley 2410 1100 V source measurement unit (Keithley Instruments Inc., Cleveland, OH, USA) and capacitance-voltage (C-V) measurement was carried out by TH2828S LCR meter (TONGHUI ELECTRONICS). All the measurements were completed at room temperature.

Results and Discussion

Deposition temperature plays a critical role in ALD technology. Figure 1a illustrates the dependences of the deposition rate and refractive index on the deposition temperature. The deposition rate constantly increases with decreasing the deposition temperature below 200 °C, which is due to the physical adsorption between the silicon substrate and the reaction precursors at the low deposition temperatures. From the profiles of refractive index as a function of deposition temperature, the constant decrease of refractive index below 200 °C means that thin films become looser, which also verifies that there is strong physical adsorption during the films'

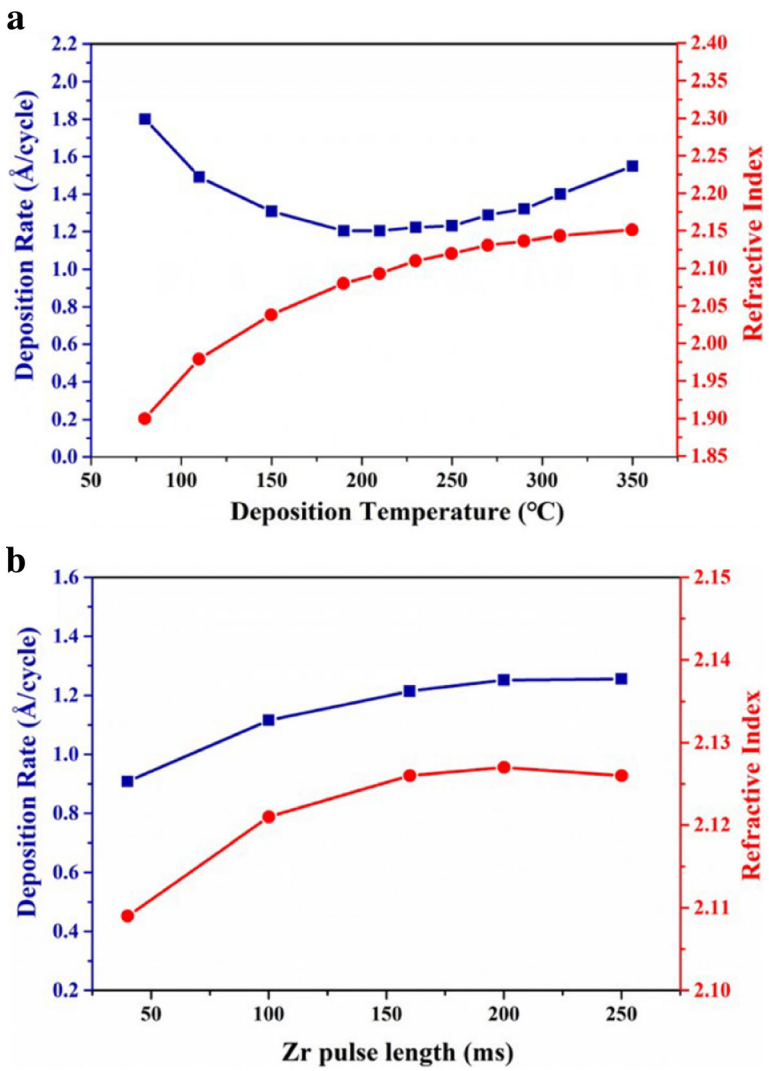

Fig. 1 The changes of deposition rate and refractive index for ZrO_2 thin films as a function of deposition temperature (**a**) and Zr precursor pulse time (**b**)

growth at the low deposition temperatures. The deposition rate of 1.25 Å/cycle can be considered as quite a stable value in the narrow temperature range of 200~250 °C, in which the chemical adsorption plays a dominant role based on saturated self-limiting surface reaction. Then the deposition rate obviously increases with increasing the deposition temperature above 250 °C. These results can be attributed to the thermal decomposition of TDMAZr at the high deposition temperatures, which leads to CVD-like deposition. Figure 1b shows the dependences of the deposition rate and refractive index on the pulse time of TDMAZr. The growth rate at about 1.25 Å/cycle is observed when pulse time is more than 200 ms, which verifies the self-limiting film growth.

Figure 2a depicts the dependence of thickness on the number of ALD cycles in ALD temperature window. The thickness of ZrO_2 films on silicon shows a linear relationship with the number of ALD cycles, and the fitted formula is $y = -1.7952 + 0.12806x$, $R = 0.99938$, which demonstrates that the thickness of thin the film can be precisely controlled by regulating the number of ALD cycles in ALD temperature window. Figure 2b shows the dependence of deposition rate on the number of ALD cycles. The deposition rate slightly increases with increasing the number of deposition cycles. Relatively low deposition rate at the beginning of film deposition can be attributed to crystal lattice mismatch and slow nucleation on silicon.

The crystallographic structure of the ZrO_2 thin films deposited at 150~350 °C was detected by GAXRD. As shown in Fig. 3a, ZrO_2 films begin to crystallize at the deposition temperature of 210 °C. The reflections at 30.5° and 35.3° are indexed to the (111) and (200) lattice

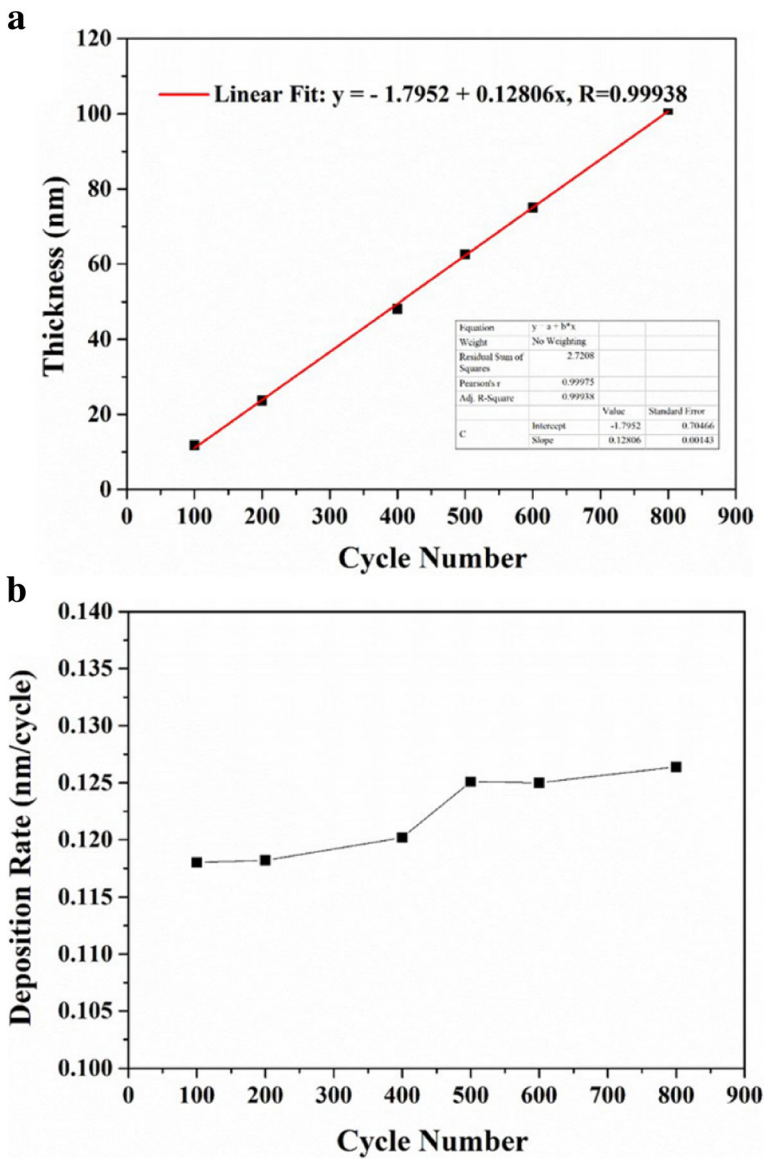

Fig. 2 The changes of thickness (**a**) and deposition rate (**b**) for ZrO_2 thin films as a function of the number of deposition cycles. The deposition temperature is 250 °C

planes of cubic phase (PDF Card 027-0997), respectively. The reflections at 51° and 60.5° are indexed to the (220) and (311) lattice planes of orthorhombic phase (PDF Card 037-1413). With increasing the deposition temperature to 290 °C, the (111), (− 111), (200), (122) and (− 131) lattice planes of stable monoclinic phase begin to appear at 28.3°, 31.4°, 35.3°, 50.6°, and 60° (PDF card 007-0343), respectively [24]. Moreover, the reflections at 30.5° and 35.3° begin to slightly shift, which indicates the phase change from cubic phases to orthorhombic phase. When the deposition temperature reaches 350 °C, the lattice planes of the cubic phase disappear, and the dominant crystallographic phases in ZrO_2 films are both orthorhombic and monoclinic phase. Post-deposition annealing is regarded as a necessary process to eliminate defects and improve the crystal quality. Figure 3b showed the GAXRD patterns of the ZrO_2 films (deposited at 250 °C) annealed at 400~1000 °C. It can be found that main crystal structures are both cubic and orthorhombic phases in the ZrO_2 film annealed at 400 °C. However, monoclinic phase begins to appear, and the intensities of reflections at 28.3° and 31.4° significantly increase with increasing annealing temperature to 1000 °C. Meanwhile, the phase change from cubic phases to orthorhombic phase can be seen from the shift of the reflection for (111) plane. From the

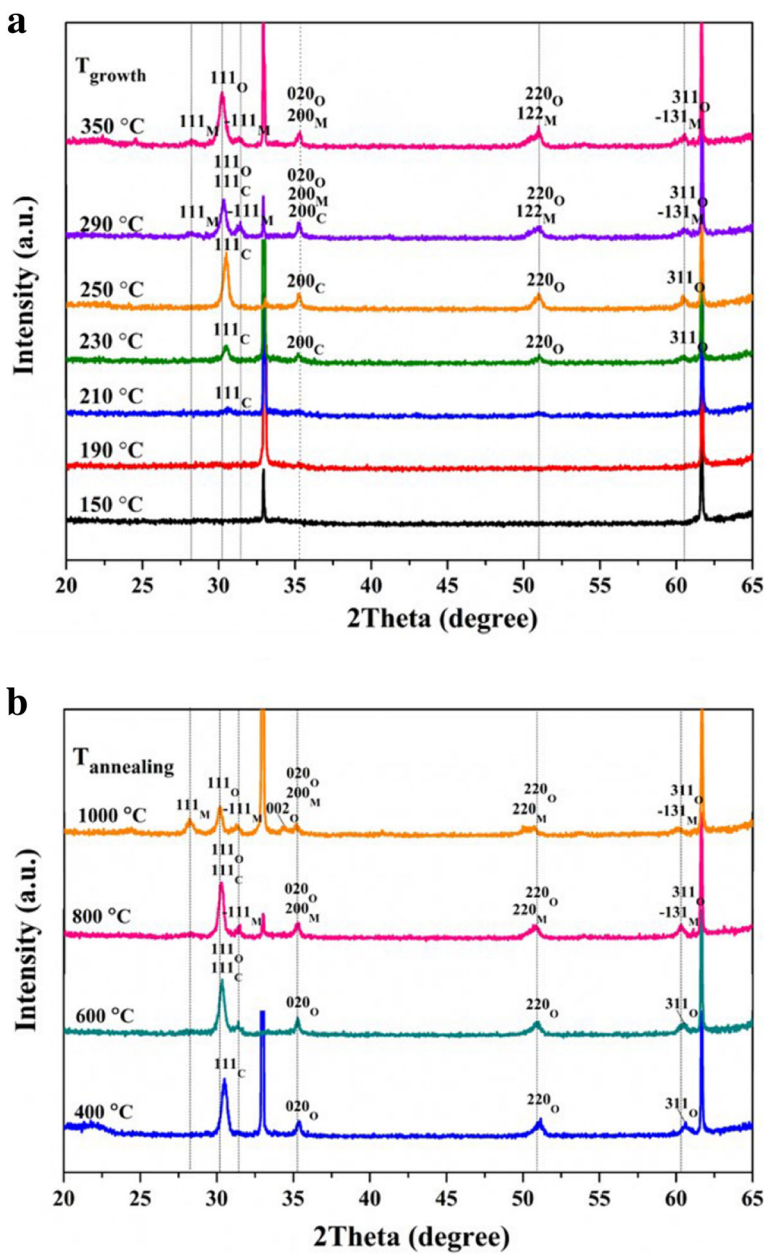

Fig. 3 The GAXRD patterns for (**a**) ZrO_2 films deposited at 150~350℃ and (**b**) ZrO_2 films annealed at 400~1000 ℃ (deposited at 250℃)

above analysis, both deposition temperature and annealing temperature have significant effects on the crystallographic structure of ZrO_2 film.

Figure 4 shows the changes of thickness and refractive index for the films deposited from 110 to 350 °C after 400 °C annealing. The thickness of the ZrO_2 film deposited below 210 °C significantly decreases after 400 °C annealing, meanwhile, the refractive index correspondingly increases, which demonstrates the thin film becomes denser after post-deposition annealing. However, the thickness and refractive index have no change for the thin film deposited above 210 °C after annealing at 400 °C, which may be because the crystal growth of thin films have been sufficient, namely, the sizes of grains are no longer obviously increase above 210 °C.

The chemical component and chemical state of ZrO_2 thin film on silicon were carefully investigated by XPS. The thickness of ZrO_2 film in XPS measurement is about 50 nm. Moreover, surface cleaning was carried out by etching before XPS measurement. As described in Fig. 5a, a full spectrum result shows the existences of oxygen and zirconium in ZrO_2 thin film deposited at

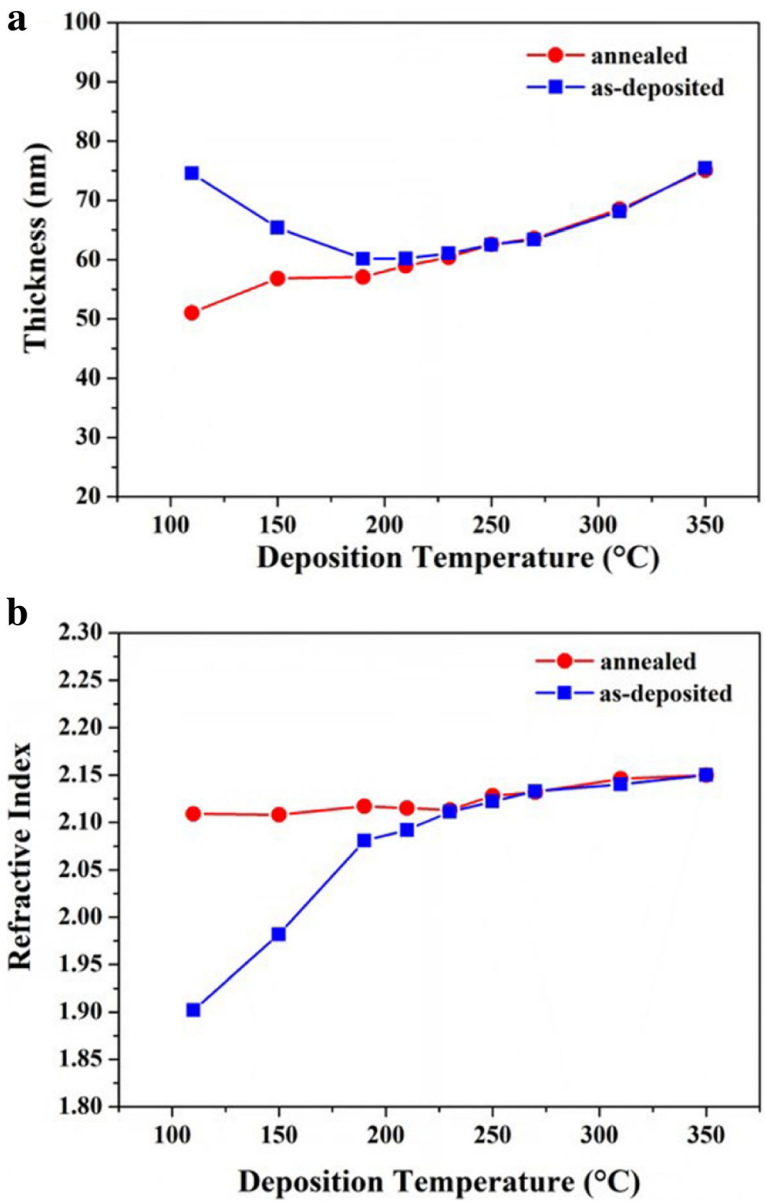

Fig. 4 The changes of thickness (**a**) and refractive index (**b**) for the films deposited at 110~350 °C after post-deposition annealing at 400 °C

250 °C, with no obvious impurity peak, which confirms the high purity of ZrO_2 thin film. Moreover, the ratio of O/Zr in ZrO_2 films deposited at 200~250 °C is 1.85–1.9, which is less than the stoichiometric ratio of ZrO_2 due to the formation of oxygen vacancy in the ZrO_2 film. An asymmetric O 1s XPS spectrum was obtained in this study, shown in Fig. 5b. The O 1s high-resolution spectrum is composed of two overlapping components, with a lower binding energy peak (529.7 eV) and the higher binding energy (531.3 eV), which result from the Zr–O of oxides and O–C of by-product, respectively. In Fig. 5c, the high-resolution spectrum of Zr 3d shows two peaks at 182.4 eV and 184.7 eV, which corresponds with the features of Zr $3d_{5/2}$ and $3d_{3/2}$, respectively. It should be noted that shoulders of the Zr $3d_{5/2}$ peak appear on the lower binding energy side. The Zr 3d spectra are decomposed satisfactorily in terms of four different oxidation states (Zr^{4+}~Zr^{+}) of Zr equally spaced in 1.06 eV (one-fourth of the chemical shift between Zr^0 and Zr^{4+}) per oxidation state with respect to the metal [32–34]. All the oxidation states are observed in all the films prepared, and the Zr^{4+} state is the major component in the films due to the effect of suboxide species. In addition, deposition temperature just has little impact on the binding energy of Zr 3d and the shape of the peaks in spectra, which demonstrates that the

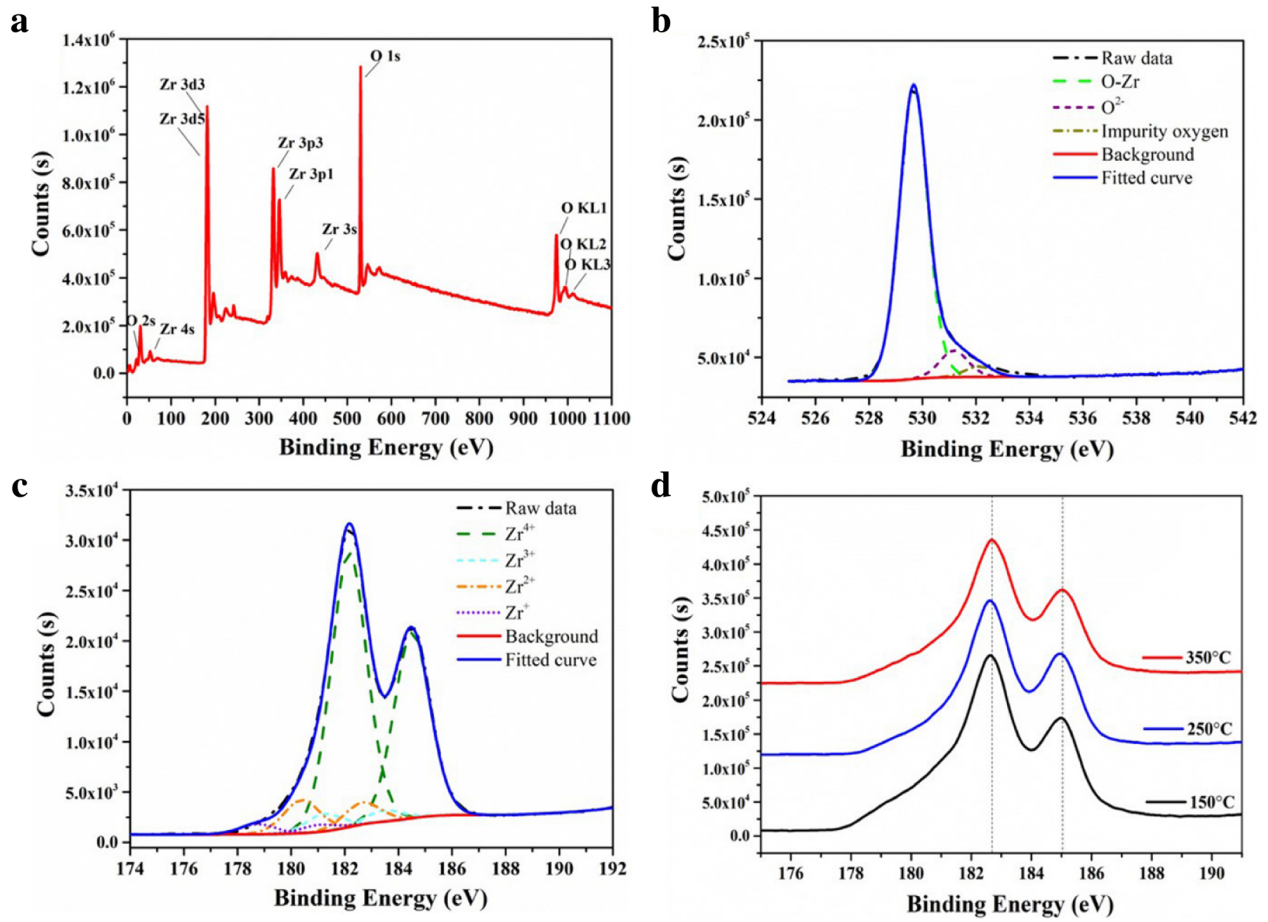

Fig. 5 The full spectrum scan of XPS (**a**), the fine spectra of O 1 s (**b**), and Zr 3d (**c**) for ZrO_2 film deposited on Si(100) at 250 °C, and the fine spectra of Zr 3d for ZrO_2 films deposited at 150, 250, and 350 °C (**d**)

deposition temperatures within the range of 150~350 °C cannot change the chemical state of Zr 3d.

Roughness and morphology were studied by AFM. Figure 6 displays representative AFM images of ZrO_2 thin films, which illustrates that the surfaces of ZrO_2 thin films are uniform and smooth. As shown in Fig. 6a and b, the root-mean-square (RMS) roughness for the ZrO_2 films deposited at 150 °C and 350 °C are 0.293 nm and 1.718 nm, which are 0.448% and 2.277% of the films aggregate thicknesses, respectively. By comparing, the result suggests that amorphous ZrO_2 films are much smoother than crystalline film. Although the RMS roughness does not provide direct evidence of the detailed evolution of crystallographic phases in oxide thin films, the increase in surface roughness could be generally ascribed to the formation and growth of the grain in the thin film. As shown in Fig. 6c and d, ZrO_2 films deposited at 250 °C were annealed at 400 °C and 1000 °C, respectively. The RMS roughness has no significant change with the increasing annealing temperature, which indicates that 400 °C annealing has led to sufficient crystal growth and there is no obvious increase in grain size. As shown in Fig. 6e and f, the thickness of ZrO_2 film controlled by ALD cycles have an obvious effect on the RMS roughness of the thin film. By comparing, the RMS roughness increases with the increasing number of ALD cycles, which can be explained by that the crystal growth is limited when the thickness of the film is very thin.

Capacitance-voltage (C-V) and current density-electric field (J-E) measurements were conducted to assess the electrical properties of MIS devices with ZrO_2 films as dielectric layers with various annealing temperatures. As shown in Fig. 7a, the capacitance constantly decreases with increasing annealing temperature. Moreover, obvious hysteresis effects between the forward and backward sweep (clockwise) were observed in the samples annealed at 400 °C and 600 °C, and then the hysteresis effect decreases or even disappears with increasing annealing temperature to 1000 °C. The hysteresis effect should be attributed to the charge trap/detrap in the interface between the ZrO_2 film and Si substrate

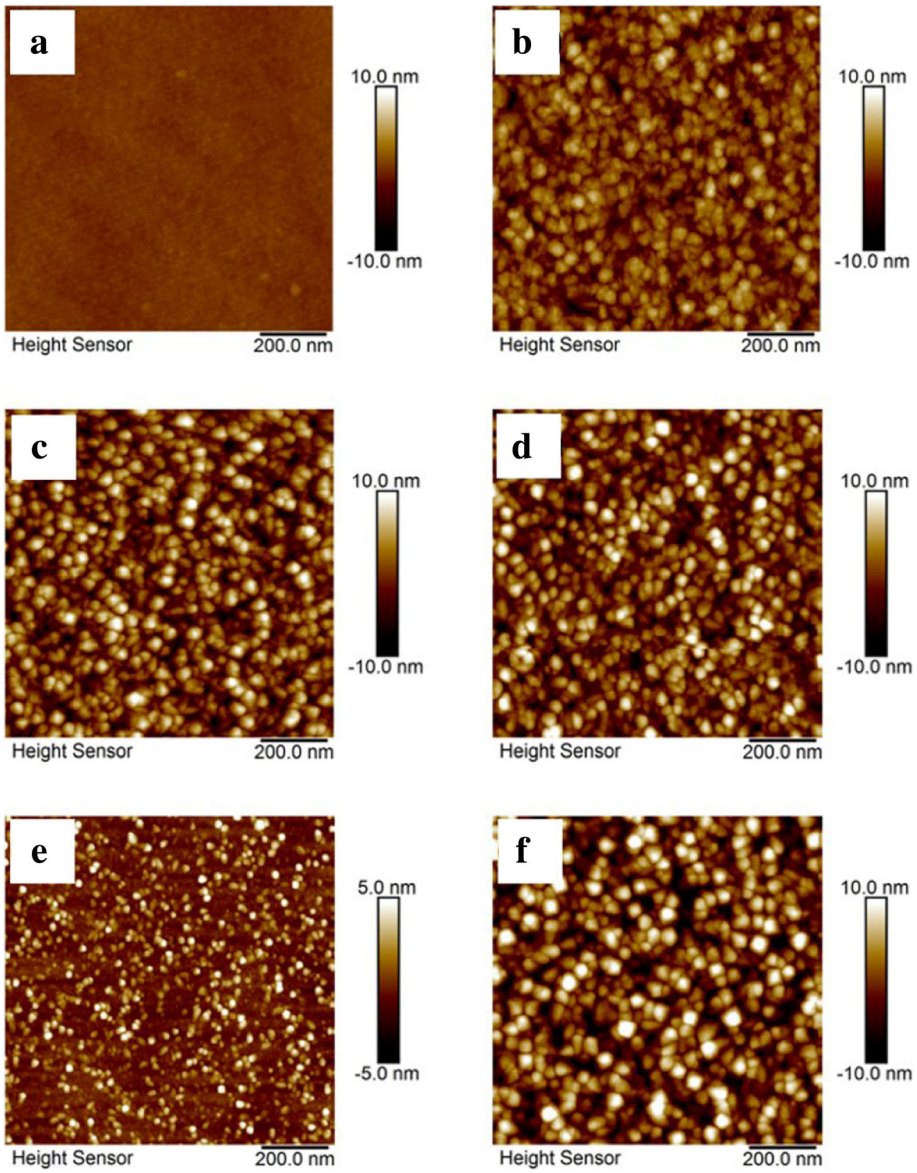

Fig. 6 AFM surface plots of ZrO_2 films deposited at 150 °C (**a**) and 350 °C (**b**), ZrO_2 films (deposited at 250 °C) annealed at 400 °C (**c**) and 1000 °C (**d**), and ZrO_2 films (deposited at 250 °C) with 200 ALD cycles (**e**) and 800 ALD cycles (**f**)

[35–37]. The oxygen in ZrO_2 film diffuses toward the interface to result in the further growth of SiO_x layer between ZrO_2 and Si substrate with increasing the annealing temperature during post-deposition annealing [37–39]. To prove the presence of SiO_x interface layer, ultrathin ZrO_2 (2.5~3 nm) deposited on Si substrate was used to XPS measurement. As shown in Fig. 8a, in Si 2p spectrum, the signal from the Si substrate (98.81 eV and 99.45 eV) could be clearly observed due to the thinness of the films, and the signal from interface layer (100.38 eV, 100.88 eV, 102.44 eV, and 103.05 eV) indicates the existence of Si sub-oxides. As shown in Fig. 8b, in the O 1s spectrum, the binding energy of 532.72 eV is identified as Si–O in SiO_x. These results can prove the formation of SiO_X interface layer. The SiO_x layer can reduce interface defect state density and improve the interface quality [39]. Therefore, the increase in annealing temperature can reduce the hysteresis effect. Figure 7b depicts J-E curves for ZrO_2-based MIS devices. With increasing the annealing temperatures from 400 °C to 800 °C, there is no significant reduction in current densities. However, with increasing the annealing temperature to 1000 °C, the leakage current density decreases to 2.85×10^{-9} A cm^{-2} at 1 MV cm^{-1}. It can be attributed to

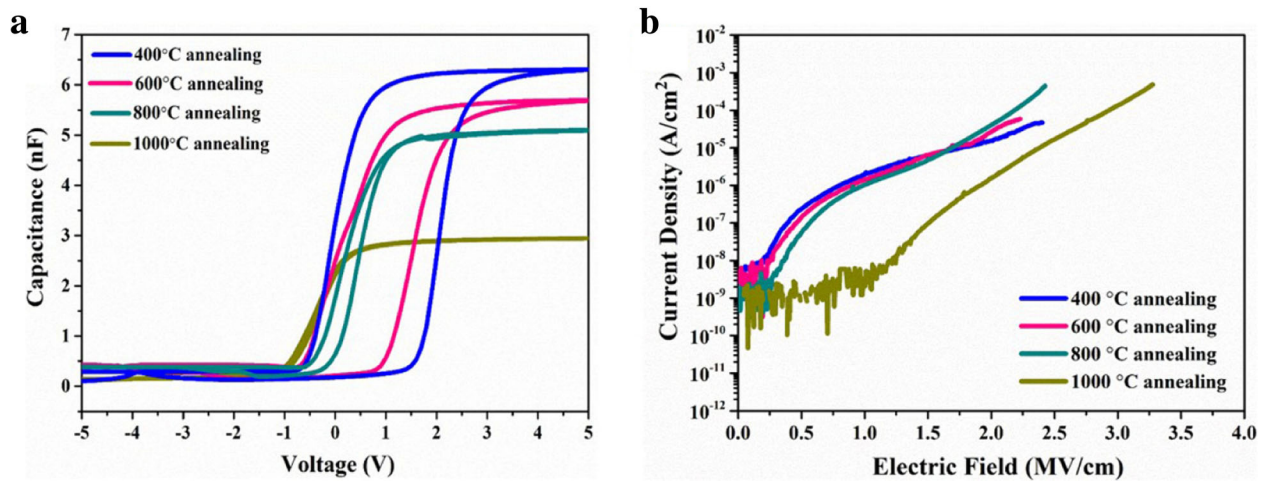

Fig. 7 The C-V (**a**) and J-E curves (**b**) for ZrO_2-based MIS devices (with 500 cycles) as a function of annealing temperature

the further growth of SiO_x intermediate layer with wide band gap during 1000 °C annealing.

Figure 9a shows the effect of ZrO_2 thickness on the capacitance behavior of ZrO_2-based MIS devices. The capacitance constantly decrease with increasing ALD cycles (or thicknesses), which is attributed to the increase in the physical thickness for ZrO_2 dielectric layer. To evaluate the dielectric constant of the ZrO_2 dielectric layer, the effect of interfacial SiO_x layer was eliminated in calculation, as shown in Fig. 10. A similar dielectric constant for ZrO_2 films with various thicknesses was obtained in Fig. 9b. The average value of the dielectric constant of ZrO_2 film is 32.57. These results indicate that the film quality is reliable for ZrO_2 films with various thickness deposited by ALD. Figure 9c and d illustrate that the increase in the physical thickness for ZrO_2 films with 400–800 ALD cycles can decrease leakage current densities. However, it should be noted that the leakage current density remains low level when the cycle number are 100 and 200, which is due to less leakage paths in the thin film with limited crystallization. As shown in Fig. 11, the GAXRD patterns for the ZrO_2 films with various ALD cycles (or thickness) illustrate the crystallization is inhibited in ZrO_2 thin film with 100 and 200 ALD cycles.

Conclusions

High-quality ZrO_2 thin films were deposited on *n*-type silicon wafers by ALD technology using tetrakis(dimethylamido)zirconium and ozone as precursors. ALD temperature window for ZrO_2 film is 200–250 °C, and

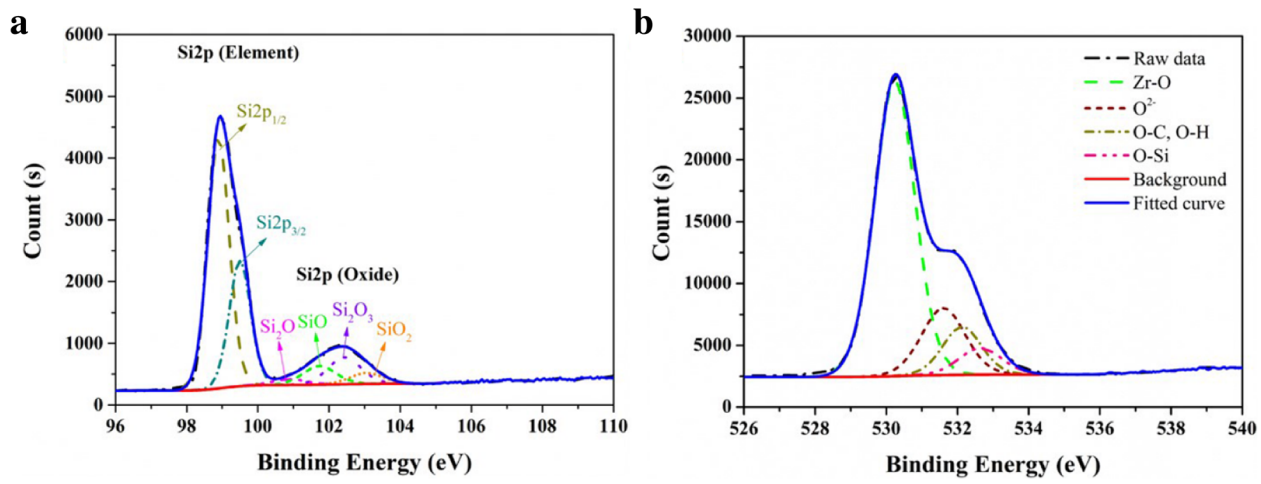

Fig. 8 The fine spectra of Si 2p and O 2s for the ZrO_2 film deposited at 250

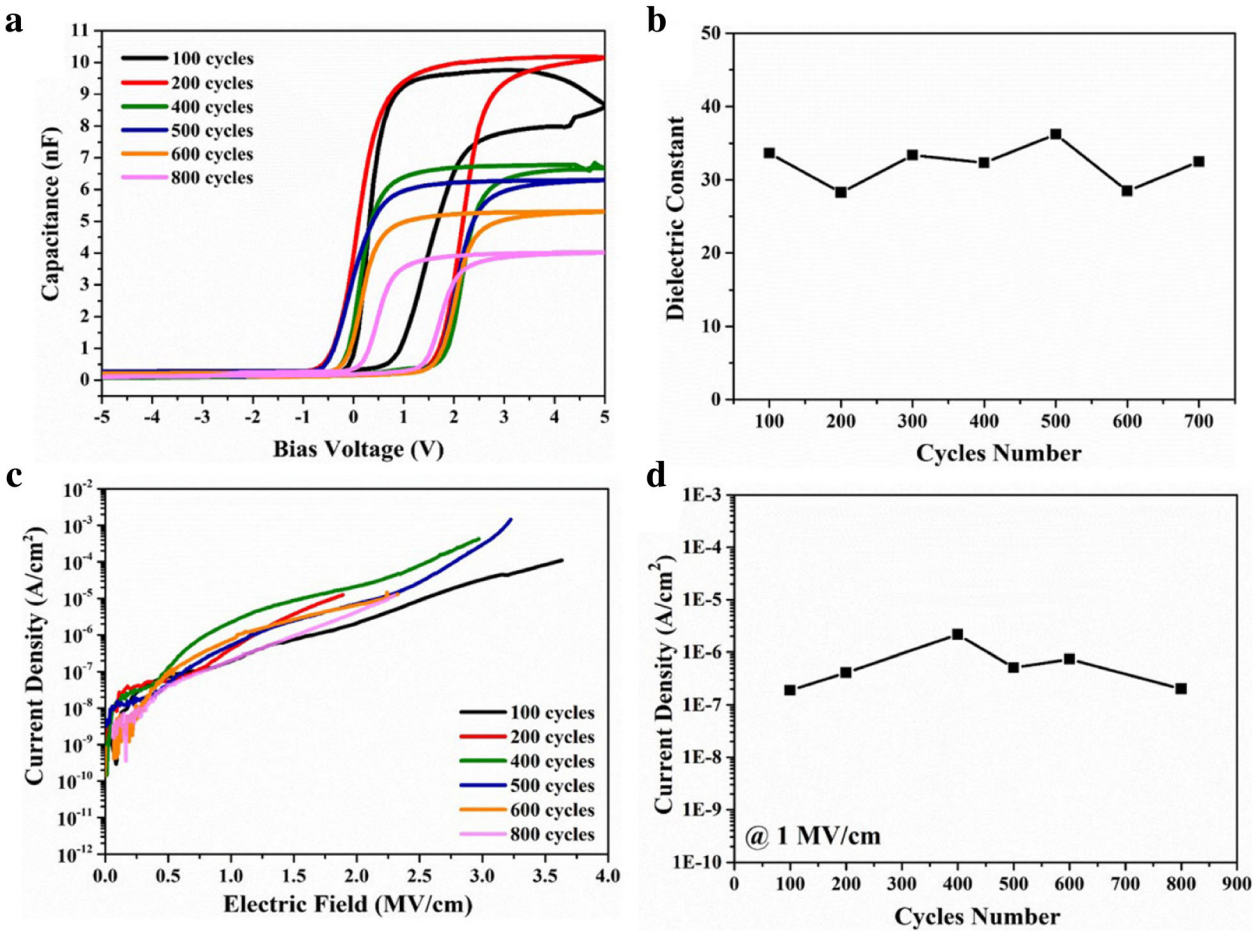

Fig. 9 The C-V (**a**) and J-E curves (**b**) for ZrO_2-based MIS devices with 100~800 cycles, the changes of dielectric constant (**c**), and the current density at 1 MV/cm (**d**) as a function of the number of deposition cycle

the deposition rate is a relatively constant at 0.125 nm/cycle. The thickness of the thin film can be precisely controlled by regulating the number of ALD cycles. The ZrO_2 films formed at 200~250 °C have an O/Zr atomic ratio of 1.85–1.9 and a low content of carbon impurity. ZrO_2 film begins to crystallize in the ALD process above 210 °C, and the crystal structure is changed from cubic and orthorhombic phases to monoclinic and orthorhombic phases with increasing the deposition temperature to 350 °C. Moreover, a similar phase transition also can occur with increasing the annealing temperature from 400 to 1000 °C. The effect of annealing temperature on

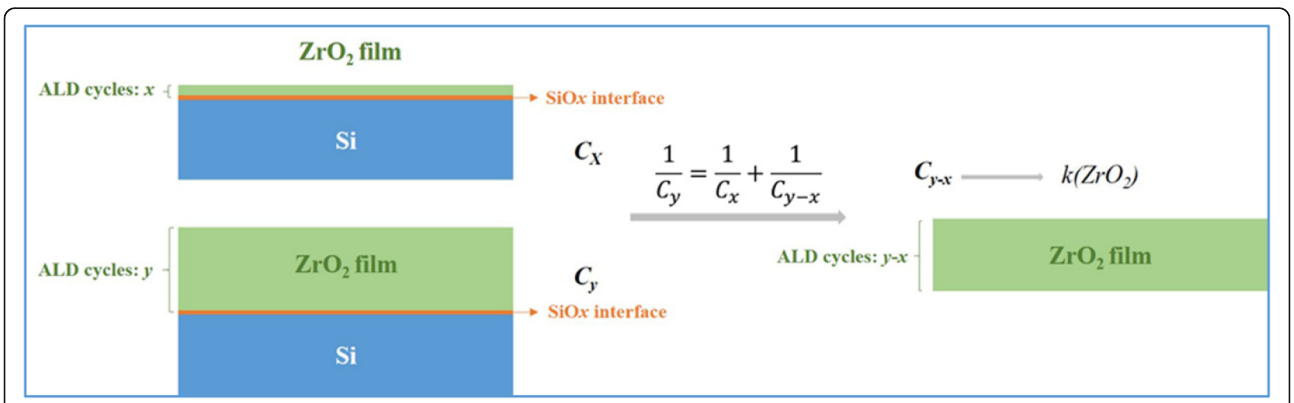

Fig. 10 Schematic diagram of dielectric constant calculation

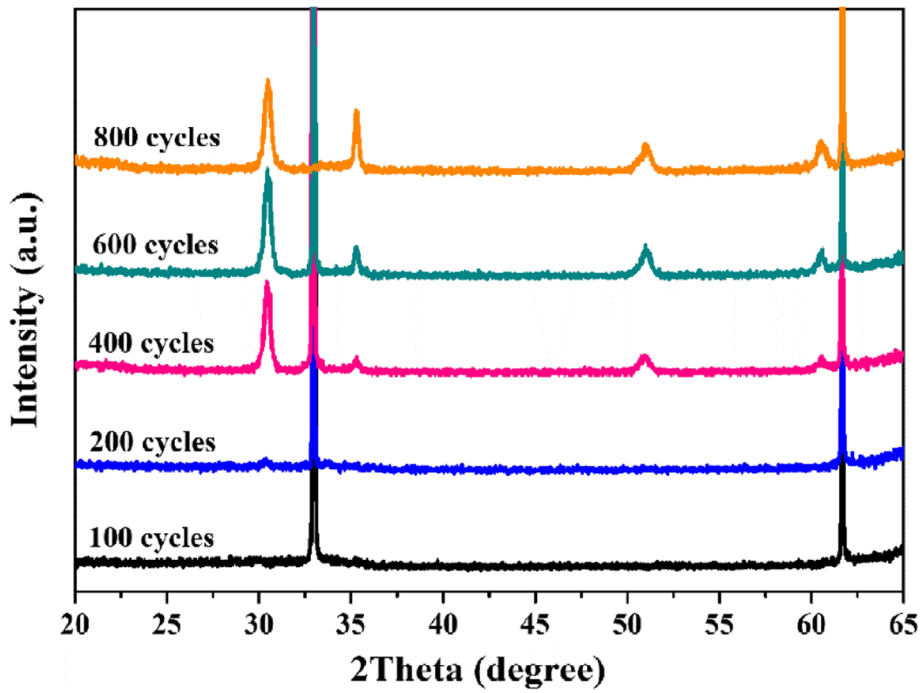

Fig. 11 The GAXRD patterns for the ZrO_2 films deposited at 250 °C with various ALD cycles

dielectric properties of ZrO_2 film was studied utilizing ZrO_2-based MIS device. The growth of the interface layer between ZrO_2 and Si substrate leads to the decrease in the capacitance and the leakage current of dielectric layer in the MIS device after 1000 °C annealing. ZrO_2 film exhibits the relatively high dielectric constant of 32.57 at 100 kHz and the low leakage current density of 3.3×10^{-6} A cm^{-2} at 1 MV/cm.

Abbreviations

AFM: Atomic force microscope; ALD: Atomic layer deposition; CMOS: Complementary metal oxide semiconductors; C-V: Capacitance-voltage; DRAM: Dynamic random access memory; I-V: Current-voltage; O_3: Ozone; RMS: Root-mean-squared; XPS: X-ray photoelectron spectroscopy; XRD: X-ray diffraction; $Zr[N(CH_3)_2]_4$: Tetrakis(dimethylamido)zirconium

Acknowledgements

This work is supported by the National Natural Science Foundation of China (no. 61674085).

Funding

National Natural Science Foundation of China (no. 61674085).

Availability of Data and Materials

All data are fully available without restriction.

Authors' Contributions

JL designed and carried out the experiments. The manuscript was written by JL. JuLi and JW took part in the C-V and I-V measurements. JS supervised the overall study. All authors read and approved the final manuscript.

Competing Interests

The authors declare that they have no competing interests.

Publisher's Note

Received: 2 December 2018 Accepted: 26 April 2019
Published online: 07 May 2019

References

1. Qi WJ, Lee BH, Nieh R, Kang LG, Jeon YJ, Onishi K, Lee JC (2004) High-k gate dielectrics. Mater Today 7:24–32
2. Bersuker G, Zeitzoff P, Brown G, Huff HR (2004) Dielectrics for future transistors. Mater Today 7:26–33
3. Robertson J (2004) High dielectric constant oxides. Eur Phys J Appl Phys 28: 265–291
4. Ye PD, Wilk GD, Yang B, Kwo J, Gossmann HJL, Hong M, Ng KK, Bude J (2004) Depletion-mode InGaAs metal-oxide-semiconductor field-effect transistor with oxide gate dielectric grown by atomic-layer deposition. Appl Phys Lett 84:434–436
5. Akatsuka K, Haga MA, Ebina Y, Osada M, Fukuda K, Sasaki T (2009) Construction of highly ordered lamellar nanostructures through Langmuir-Blodgett deposition of molecularly thin titania nanosheets tens of micrometers wide and their excellent dielectric properties. ACS Nano 3: 1097–1106
6. Robertson J, Wallace RM (2015) High-K materials and metal gates for CMOS applications. Mater Sci Eng R 88:1–41
7. Chen W, Ren W, Zhang Y, Liu M, Ye ZG (2015) Preparation and properties of ZrO_2 and TiO_2 films and their nanolaminates by atomic layer deposition. Ceram Int 41:S278–S282
8. Copel M, Gribelyuk M, Gusev E (2000) Structure and stability of ultrathin zirconium oxide layers on Si (001). Appl Phys Lett 76:436–438
9. Qi WJ, Nieh R, Lee BH, Kang L, Jeon Y, Lee JC (2000) Electrical and reliability characteristics of ZrO_2 deposited directly on Si for gate dielectric application. Appl Phys Lett 77:3269–3271
10. Kukli K, Ritala M, Leskelä M (2000) Low-temperature deposition of zirconium oxide-based nanocrystalline films by alternate supply of $Zr[OC(CH_3)_3]_4$ and H_2O. Chem Vap Depos 6:297–302
11. Ye G, Wang H, Arulkumaran S, Ng GI, Hofstetter R, Li Y, Anand MJ, Ang KS, Maung YKT, Foo SC (2013) Atomic layer deposition of ZrO as gate

dielectrics for AlGaN/GaN metal-insulator-semiconductor high electron mobility transistors on silicon. Appl Phys Lett 103:142109
12. Chang JP, Lin YS (2001) Dielectric property and conduction mechanism of ultrathin zirconium oxide films. Appl Phys Lett 79:3666–3668
13. Majedi A, Davar F, Abbasi A, Ashrafi A (2016) Modified sol–gel based nanostructured zirconia thin film: preparation, characterization, photocatalyst and corrosion behavior. J Inorg Organomet Polym Mater 26:1–11
14. Woods KN, Chiang TH, Plassmeyer PN, Kast MG, Lygo AC, Grealish AK, Boettcher SW, Page CJ (2017) High-k lanthanum zirconium oxide thin film dielectrics from aqueous solution precursors. ACS Appl Mater Interfaces 9: 10897–10903
15. Brenier R, Gagnaire A (2001) Densification and aging of ZrO_2 films prepared by sol-gel. Thin Solid Films 392:142–148
16. George SM (2010) Atomic layer deposition: an overview. Chem Rev 110: 111–131
17. Niinistö J, Kukli K, Heikkilä M, Ritala M, Leskelä M (2010) Atomic layer deposition of high-k oxides of the group 4 metals for memory applications. Adv Eng Mater 11:223–234
18. Zhang Y, Ren W, Jiang Z, Yang S, Jing W, Shi P, Wu X, Ye ZG (2014) Low-temperature remote plasma-enhanced atomic layer deposition of graphene and characterization of its atomic-level structure. J Mater Chem C 2:7570–7574
19. Gieraltowska S, Wachnicki L, Witkowski BS, Mroczynski R, Dluzewski P, Godlewski M (2015) Characterization of dielectric layers grown at low temperature by atomic layer deposition. Thin Solid Films 577:97–102
20. Kukli K, Forsgren K, Ritala M, Leskelä M, Aarik J, Haårsta A (2001) Dielectric properties of zirconium oxide grown by atomic layer deposition from iodide precursor. J Electrochem Soc 148:F227–F232
21. Kukli K, Ritala M, Aarik J, Uustare T, Leskela M (2002) Influence of growth temperature on properties of zirconium dioxide films grown by atomic layer deposition. J Appl Phys 92:1833–1840
22. Putkonen M, Niinistö J, Kukli K, Sajavaara T, Karppinen M, Yamauchi H, Niinistö L (2010) ZrO_2 thin films grown on silicon substrates by atomic layer deposition with $Cp_2Zr(CH_3)_2$ and water as precursors. Chem Vap Depos 9: 207–212
23. Lamperti A, Lamagna L, Congedo G, Spiga S (2011) Cubic/tetragonal phase stabilization in high-κ ZrO_2 thin films grown using O_3-based atomic layer deposition. J Electrochem Soc 158:G221–G226
24. Kukli K, Kemell M, Köykkä J, Mizohata K, Vehkamäki M, Ritala M, Leskelä M (2015) Atomic layer deposition of zirconium dioxide from zirconium tetrachloride and ozone. Thin Solid Films 589:597–604
25. Kukli K, Forsgren K, Aarik J, Uustare T, Aidla A, Niskanen A, Ritala M, Leskelä M, Hårsta A (2001) Atomic layer deposition of zirconium oxide from zirconium tetraiodide, water and hydrogen peroxide. J Cryst Growth 231: 262–272
26. Van TT, Bargar JR, Chang JP (2006) Er coordination in Y_2O_3 thin films studied by extended x-ray absorption fine structure. J Appl Phys 100:023115
27. Aarik J, Aidla A, Mändar H, Sammelselg V, Uustare T (2000) Texture development in nanocrystalline hafnium dioxide thin films grown by atomic layer deposition. J Cryst Growth 220:105–113
28. Tsyganova EI, Dyagileva LM, Aleksandrov YA (1999) Thermal stability of zirconium organic derivatives with ligands of different nature. Russ J Gen Chem 69:1532–1535
29. Mol AMBV, Driessen JPAM, Linden JL, Croon MHJMD, Spee CIMA, Schouten JC (2001) Vapor pressures of precursors for the CVD of titanium nitride and tin oxide. Chem Vap Depos 7:101–104
30. Hausmann DM, Kim E, Jill Becker A, Gordon RG (2012) Atomic layer deposition of hafnium and zirconium oxides using metal amide precursors. Chem Mater 14:4350–4358
31. Duan Y, Sun F, Yang Y, Chen P, Yang D, Duan Y, Wang X (2014) Thin-film barrier performance of zirconium oxide using the low-temperature atomic layer deposition method. ACS Appl Mater Interfaces 6:3799–3804
32. Morant C, Sanz JM, Galán L, Soriano L, Rueda F (1989) An XPS study of the interaction of oxygen with zirconium. Surf Sci 218:331–345
33. González COD, García EA (1988) An X-ray photoelectron spectroscopy study of the surface oxidation of zirconium. Surf Sci 193:305–320
34. Matsuoka M, Isotani S, Miyake S, Setsuhara Y, Ogata K, Kuratani N (1996) Effects of ion energy and arrival rate on the composition of zirconium oxide films prepared by ion-beam assisted deposition. J Appl Phys 80:1177–1181
35. Lin J, Gomeniuk YY, Monaghan S, Povey IM, Cherkaoui K, O'Connor E, Power M, Hurley PK (2013) An investigation of capacitance-voltage hysteresis in metal/high-k/$In_{0.53}Ga_{0.47}$ as metal-oxide-semiconductor capacitors. J Appl Phys 114:1295–1496
36. Zhao CZ, Taylor S, Chalker PR, Jones AC, Zhao C (2011) Dielectric relaxation of La-doped zirconia caused by annealing ambient. Nanoscale Res Lett 6: 48–48
37. Nakajima A, Kidera T, Ishii H, Yokoyama S (2002) Atomic-layer deposition of ZrO_2 with a Si nitride barrier layer. Appl Phys Lett 81:2824–2826
38. Sang YL, Kim HK, Lee JH, Yu IH, Lee JH, Hwang CS (2014) Effects of O_3 and H_2O as oxygen sources on the atomic layer deposition of HfO_2 gate dielectrics at different deposition temperatures. J Mater Chem C 2:2558–2568
39. Kukli K, Ritala M, Leskelä M, Sajavaara T, Keinonen J, Gilmer DC, Hegde R, Rai R, Prabhu L (2003) Atomic layer deposition of HfO_2 thin films and nanolayered HfO_2–Al_2O_3–Nb_2O_5 dielectrics. J Mater Sci Mater El 14:361–367